

Möbius boron–nitride nanobelts interacting with heavy metal nanoclusters

C. Aguiar¹, N. Dattani^{2,3}, I. Camps^{1,3*}

¹*Laboratório de Modelagem Computacional - LaModel, Instituto de Ciências Exatas - ICEX. Universidade Federal de Alfenas - UNIFAL-MG, Alfenas, Minas Gerais, Brasil*

²*HPQC College, Waterloo, Canada*

³*HPQC Labs, Waterloo, Canada*

Abstract

How do nickel, cadmium, and lead nanoclusters interact with boron-nitride and Möbius-type boron-nitride nanobelts? To answer this question, we used the semiempirical tight binding framework, as implemented in the xTB software, to determine the lowest energy geometries, binding energy, complexes stability, and electronic properties. Our calculations show that heavy metal nanoclusters favorably bind to both boron-nitride nanobelts, although the interaction is stronger with the Möbius-type nanobelt. The calculations show that the nickel nanocluster has the lowest binding energy and the greatest charge transfer with the nanobelts, followed by the cadmium and lead nanoclusters. During the simulation time, the molecular dynamic simulation showed that all complexes were stable at 298 K. Following the nanobelt's symmetry, the frontier orbitals are distributed homogeneously throughout the structure. This distribution changed when the nanobelt was twisted to create the Möbius-type nanobelt. The topological study indicated that the number of bonds between the metal nanoclusters and the Möbius-type nanobelt doubled and that the bonds formed with the nickel nanocluster were stronger than those formed with the cadmium and lead metals. Combining all the results, we conclude that the nickel nanoclusters are chemisorbed, whereas the cadmium and lead nanoclusters are physisorbed in both nanobelts.

Keywords: heavy metals, boron nitride nanobelt, Möbius belt, Nickel, Cadmium, Lead

1. Introduction

Industrialization and population growth have significantly contributed to the increase in pollution [1; 2]. Heavy metal ions, when released into the environment, can cause numerous diseases such as cancer, hepatitis, spontaneous abortions, anemia, among others [3; 4]. Lead (Pb), for example, is a carcinogenic element and its toxicity can cause mental retardation, congenital defects, brain damage, and death [5]. Nickel ions (Ni) can cause skin diseases [6]. Cadmium (Cd) is not only carcinogenic but can also cause damage to the kidneys and respiratory system [7; 8]. This is because these metals have no biological function, but can accumulate and interfere with metabolism and physiological processes [8]. Therefore, prevention, as well as the identification and treatment of pollutants, are essential for the maintenance and preservation of the environment. In this sense, nanotechnology can play a fundamental role in identifying and treating effluents [8; 9].

Nanocarbon materials, due to their large surface area, have mesopores that make them ideal for removing heavy metal ions through adsorption [8; 10; 11]. Moreover, these nanomaterials can be functionalized with numerous molecules that can make them specific to adsorb certain materials [8; 12]. Carbon nanostructures have already been reported for use in heavy metal adsorption and are also used in purifying water contaminated with heavy metals [8; 11; 13–16]. In addition, it is reported that the adsorbed metal ions can be easily desorbed, and the nanomaterials can be recycled and reused [8]. Furthermore, carbon-based nanomaterials are highly biocompatible with living organisms and the environment [17].

When carbon atoms are replaced by boron and nitrogen atoms, boron nitride nanotubes (BNNTs) are obtained [18]. With an identical structure to carbon nanotubes, BNNTs have similar mechanical properties [18; 19] and they are electrically insulating, with a forbidden band between 5.0–6.0 eV, independent of chirality [18; 20]. In addition, the thermal properties are improved due to boron nitride (BN) having high atmospheric stability, especially at high temperatures [21]. This makes BNNT an excellent candidate for applications

*Corresponding authors

Email addresses: nike@hpqc.org (N. Dattani^{2,3}), icamps@unifal-mg.edu.br (I. Camps^{1,3})

in electronics [22], sensors [23], hydrogen storage [24], medicine [25; 26], and also water purification [15; 16; 27–30] among others.

Due to these particularities, research on a new structure has been investigated, the boron nitride nanobelts (BN-nanobelts), an inorganic analog of cyclofenacene synthesized in 2017 [31; 32]. Aromatic BN-nanobelts have radially oriented p orbitals with photoluminescent properties and excellent UV absorber, suggesting that this molecule can be used as a UV detector [32–34]. In addition, BN-nanobelts have high chemical stability, thermal stability with positive vibrational frequencies and insulating character with an estimated gap of around 5 eV [32; 35]. Considering this, properties originating from these different topologies can help solve current problems such as pollution caused by undesirable chemical contaminants that cause adverse effects on nature and living organisms [8; 9]. Contamination by heavy metal ions, mainly in water resources, is a serious environmental problem.

In this study, the interaction of Cadmium (Cd), Nickel (Ni), and Lead (Pb), with boron–nitride and Möbius-type boron–nitride nanobelts were investigated using the semiempirical tight binding theory. Several methods were used to characterize the systems: best interaction region detection, geometry optimization, molecular dynamics, electronic property calculations, and topology studies.

2. Materials and Methods

In this work, three heavy metals (Cd, Ni, and Pb) were used, together with two different types of boron-nitride (BN) nanostructures.

The metals considered here are in the form of four–atom nanoclusters (M4). We considered a one-dimensional linear chain (1DL, Figure 1(a)), a one-dimensional zigzag chain (1DZ, Figure 1(b)), a two-dimensional plane (2D, 1(c)), and a three-dimensional tetrahedron (3D, 1(d)).

Two types of BN nanostructures were considered: one consisting of a nanobelt (NB) and the other consisting of a Möbius nanobelt (twisted nanobelt). The structures were generated using the Virtual NanoLab Atomistix Toolkit software [36] as follows. We started with 2 unit cells of (10,0) boron-nitride nanosheet repeated 10 times in the z direction and then

wrapped 360 degrees. After that, the periodicity was removed, and the border atoms were passivated with hydrogen. In the case of Möbius nanobelts, after the initial repetition of the cells, the nanobelt was twisted 180 degrees and then wrapped. Both nanostructures are shown in Figure 2.

In order to clearly identify the systems, the following nomenclature was used: BNNB for boron-nitride nanobelt, MBNNB for Möbius boron-nitride nanobelt, and BNNB+M4 (MBNNB+M4) for the complexes formed by the BNNB (MBNNB) and the metal cluster, M4.

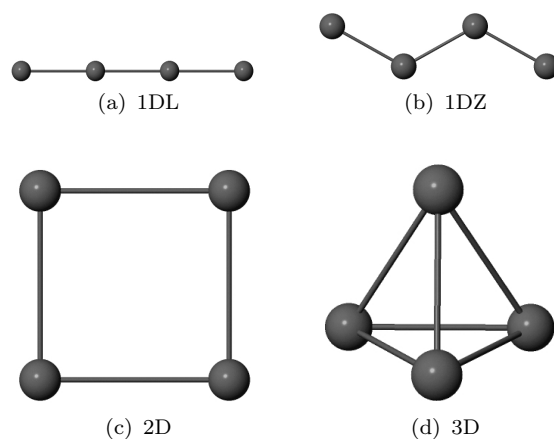


Figure 1: Nanoclusters geometry: (a) one dimensional linear chain (1DL), (b) one dimensional zigzag chain (1DZ), (c) two dimensional plane (2D), and (d) three dimensional tetrahedron (3D).

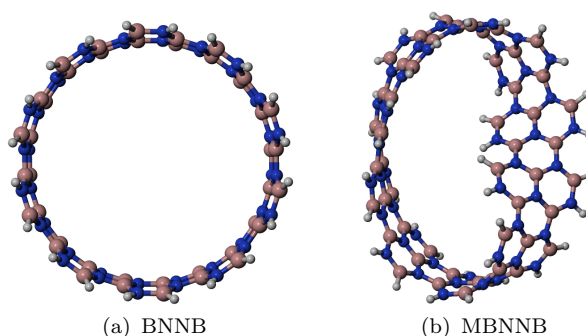


Figure 2: (a) Boron-nitride nanobelt (BNNB). (b) Möbius boron-nitride nanobelt (MBNNB).

To perform the calculations, we used the semiempirical tight binding method, as implemented in the xTB program [37; 38]. The calculations were done following a series of steps

described below.

First, we optimized the structures of each individual system (two nanobelts and four nanoclusters for each metal). Then, using the automated Interaction Site Screening (aISS) [39], we generated different intermolecular geometries (e.g., BNNB+M4 and MBNNB+M4) and subjected them to further genetic optimization. We used the interaction energy (xTB-*IFF*) [40] of each newly generated structure for ranking, and the genetic step was repeated ten times until the best complex was obtained. The best-ranked complexes were further subjected to structural optimization. In order to study the complexes' stability, each structure obtained in the aISS step was subjected to a molecular dynamic (MD) simulation for a period of 100 ps.

All geometry optimizations were performed using the GFN2-xTB method, which is an accurate self-consistent method that includes multipole electrostatics and density-dependent dispersion contributions [41]. Extreme optimization level was ensured, with a convergence energy of $5 \times 10^{-8} E_h$ and gradient norm convergence of $5 \times 10^{-5} E_h/a_0$ (where a_0 is the Bohr radius). MD simulations were also conducted using the GFN2-xTB method.

The electronic properties calculated included the system energy, the energy of the highest occupied molecular orbital (HOMO) (ε_H), the energy of the lowest unoccupied molecular orbital (LUMO) (ε_L), the energy gap between HOMO and LUMO orbitals ($\Delta\varepsilon = \varepsilon_H - \varepsilon_L$), and the atomic charges using the CM5 scheme [42].

From the calculated charges, we estimated the charge transfer between the isolated metal nanocluster and the nanobelts using the expression

$$\Delta Q_{M4} = Q_{M4}^{ads} - Q_{M4}^{iso}, \quad (1)$$

where Q_{M4}^{ads} is the total charge on the metal nanocluster after adsorption, and Q_{M4}^{iso} is the total charge for the isolated metal nanocluster.

The binding energies (E_b) of the adsorbed metals on the nanobelts were calculated using

the following expression

$$E_b = E_{NB+M4} - E_{NB} - E_{M4}. \quad (2)$$

In equation 2, E_{NB} and E_{M4} are the energies for the isolated nanobelts and metal nanoclusters, respectively, and E_{NB+M4} is the energy of the NB+M4 complex (BNNB+M4 and MBNNB+M4 systems).

Finally, the topological characterization was carried out using the MULTIWFN [43] software, where the topological properties such as critical points, critical path, basins, etc. were determined for each complex.

3. Results and discussion

3.1. Nanoclusters adsorption at the BN nanobelts

Figure 3 shows the fully relaxed structures, with the point of view being the same as in Figure 2. Only the complexes with the lowest final energy for each metal are displayed. For BNNB, the Cd1DL, Ni1DZ, and Pb2D nanoclusters had the lowest energy complexes. The MBNNB behaved similarly for cadmium and lead, but for nickel, the optimal structure was with the Ni2D cluster. At first sight, the interaction with nickel nanoclusters deforms the nanobelts to a greater extent than the other metals and also forms more bonds. Both behaviors may indicate greater binding between BNNB and MBNNB with Ni.

A significant contrast between chemisorption and physisorption is the effect on the electronic states of both the adsorbate and the adsorbent [45]. We will observe in sections 3.2 and 3.3 that the electronic properties of the systems are altered upon adsorption, confirming this phenomenon.

Table 1 displays the data for the complexes with the lowest energy. Two binding energies are reported: E_b^{aISS} and E_b . The former is obtained from the aISS step, while the latter is calculated using equation 2 for the fully optimized individual structures and final complex. Comparing both binding energies for each system, the Ni clusters have the lowest binding

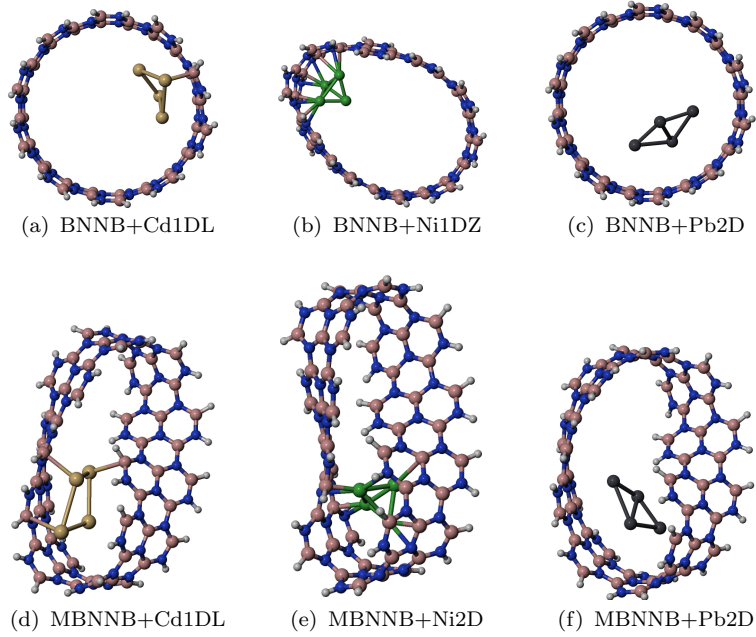


Figure 3: Fully relaxed complexes with lowest energies. Image rendered with Jmol software [44].

Table 1: Data from geometry optimization and electronic calculation[†].

Complex	E_b^{aISS}	E_b	ΔQ_M	Gap ($\Delta\varepsilon$)	Distances
BNNB+Cd1DL	-95.33	-82.87	0.0622	0.999	2.48/3.03/3.18/3.23/3.32/3.54
BNNB+Ni1DZ	-142.77	-116.01	-0.1195	0.144	2.24/2.27/2.32/2.44
BNNB+Pb2D	-93.36	-54.31	0.0014	1.226	3.51/3.53/3.71
MBNNB+Cd1DL	-109.25	-96.78	0.0085	0.826	2.59/2.68/2.85/2.88/2.90/3.38 3.39/3.41/3.58/3.69/3.83/3.92
MBNNB+Ni2D	-163.68	-149.83	-0.2223	0.109	2.15/2.21/2.52/2.57/2.70/2.71/3.60
MBNNB+Pb2D	-99.00	-59.98	0.0248	1.449	2.81/2.92/3.31/3.37/3.61/4.41

[†] E_b^{aISS} and E_b are in units kcal/mol, ΔQ_M are in units of e , $\Delta\varepsilon$ is in units of eV and the distances are in \AA , respectively.

energies, indicating stronger adsorption, followed by Cd and Pb. As all the binding energies are negative, all the adsorption processes are favorable.

The graphical representation of the complexes in Figure 3 suggests that only Cd and Ni formed bonds with the nanobelts. In the case of Cd, it made one bond with BNNB and two bonds with MBNNB. The Ni cluster formed ten bonds with BNNB and eight with MBNNB, whereas Pb did not make any bonds with either BNNB or MBNNB. Since the bond information from Figure 3 is only based on geometrical data, the Quantum Theory of Atoms in Molecule (QTAIM) [46] was used in Section 3.3 as a more accurate method to study bond formation.

Geometry optimization involves using an algorithm to obtain a local minimum structure on the potential energy surface (PES), which allows us to determine the lowest energy conformers of a system. However, this method provides no information about the system's stability over time. Molecular dynamics simulation, on the other hand, analyzes the movement of atoms and molecules at a specific temperature (here, 298.15 K) and provides a way to explore the PES. We used this method to perform simulations on each complex, starting with the structures obtained from the aISS step as initial conformations. The simulations were run for a production time frame of 100 ps with a time step of 2 fs and an optional dump step of 50 fs, at which the final structure was written to a trajectory file.

Figures 4 and 5 show the system frames at several simulation times (0 ps, 25 ps, 50 ps, 75 ps, and 100 ps). In all cases, the metal nanoclusters remained bound to their respective BN nanobelts, indicating system stability. By comparing the snapshots from figures 4 and 5 with Figure 2, we confirmed that the Ni nanocluster caused the most significant modifications to the nanobelt. The full molecular dynamics movies can be downloaded from the Zenodo server [47].

3.2. *Electronic properties*

Figures 6 and 7 show the calculated highest occupied/lowest unoccupied molecular orbitals (HOMO/LUMO) for all optimized systems.

The molecular orbitals for the BNNB system (Figures 6(a) and 7(a)) are homogeneously

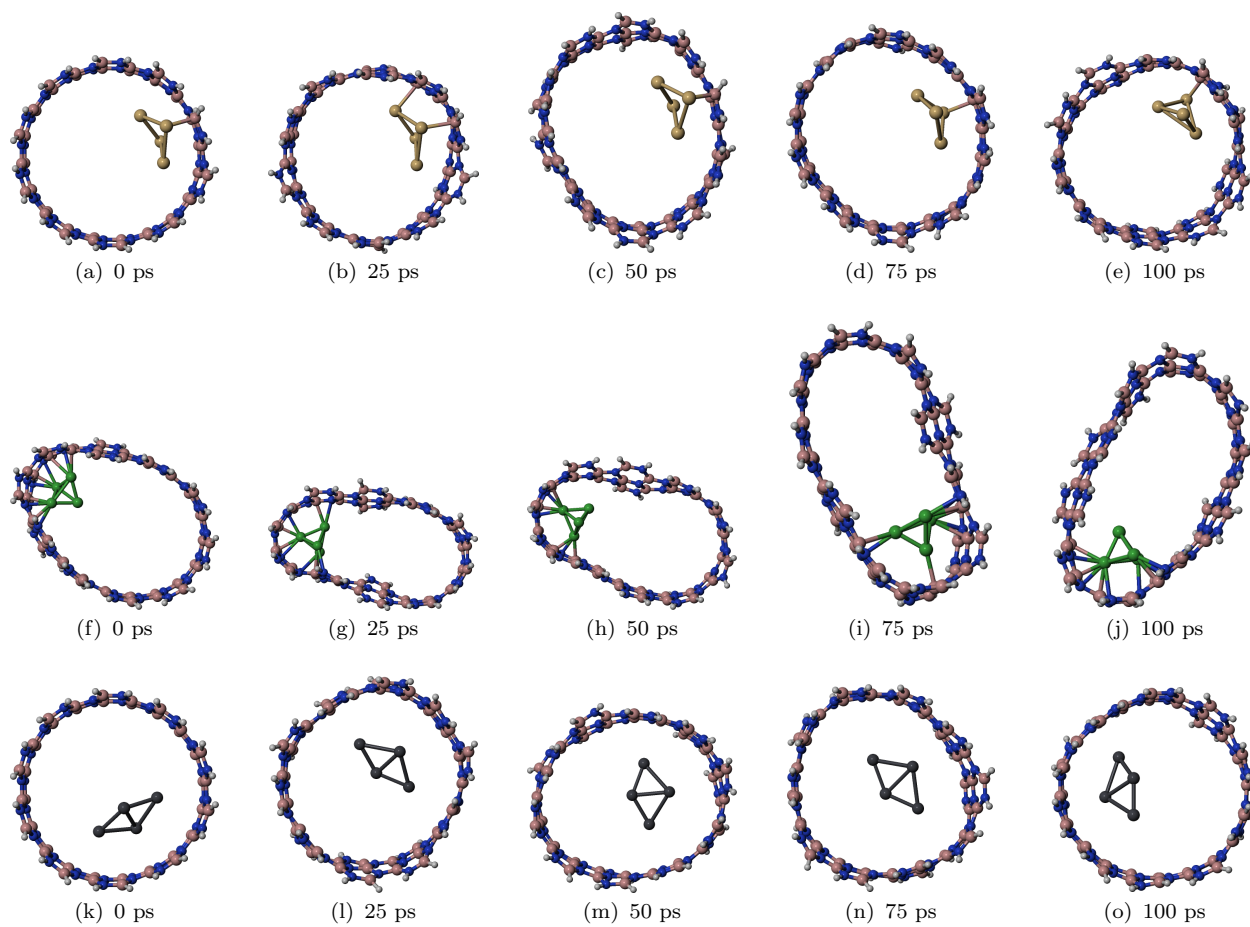


Figure 4: Molecular dynamics snapshots at different simulation times for BNNB complexes. Simulation times (from left to right): 0 ps, 25 ps, 50 ps, 75 ps and 100 ps, respectively. And systems (from top to bottom): BNNB+Cd1DL, BNNB+Ni1DZ and BNNB+Pb2D, respectively.

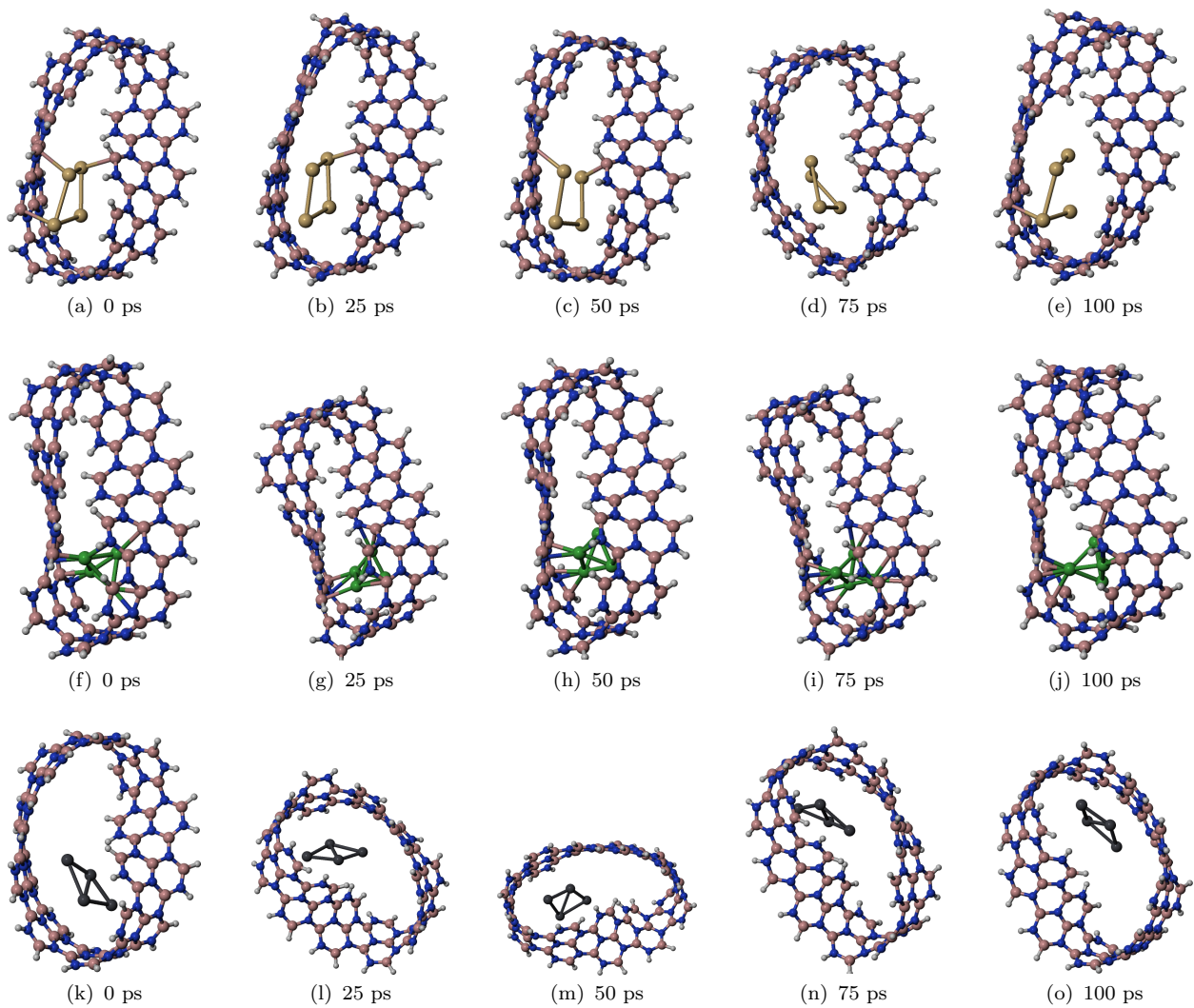


Figure 5: Molecular dynamics snapshots at different simulation times for MBNNB complexes. Simulation times (from left to right): 0 ps, 25 ps, 50 ps, 75 ps and 100 ps, respectively. And systems (from top to bottom): MBNNB+Cd1DL, MBNNB+Ni2D and MBNNB+Pb2D, respectively.

distributed over the entire structure, as expected due to the belt symmetry. These distributions change when the nanobelts are twisted, breaking their symmetry (figures 6(e) and 7(e)). In the Möbius nanobelt, there is a redistribution of both molecular orbital surfaces, with more volume concentrated around the regions with the twist, especially for the HOMO. The electronic gap for the BNNB is equal to 3.973 eV, which is slightly decreased to 3.859 eV for the MBNNB.

In the case of the complexes, the interaction with the heavy metal nanoclusters greatly modifies the HOMO for all systems, with the orbital volume becoming more concentrated around the metal adsorption regions. A similar behavior occurs for the LUMO, but to a greater extent for Ni and Pb than for Cd. The gap for the complexes is also modified after adsorption, with the greatest change observed for Ni, followed by Cd and Pb. The interaction of both nanobelts with all the metals decreases the gap, as shown in Table 1. Again, the interaction with Ni induced the greatest change in the electronic gap.

Another indicator of adsorption strength is the charge transfer (ΔQ_{M4}) between the adsorbent and adsorbate. The ΔQ_{M4} was calculated using the equation 1 and its value is shown in Table 1 for all systems. In both cases (BNNB and MBNNB), the greatest charge transfer occurs between the nanobelts and the Ni nanocluster.

Based on the intensity of the modifications in the electronic properties of the BNNB and MBNNB after interaction with metals, we can conclude that chemisorption occurs for all systems. This conclusion from the analysis of electronic properties will be confirmed by the topological studies presented in the next section.

3.3. Topological analysis

In topological analysis, a key objective is to identify critical points. These critical points (CPs) are points where the gradient norm of the function value is zero, and they are classified into four types based on the negative eigenvalues of the Hessian matrix of the real function [46].

When three eigenvalues of the Hessian matrix are negative, the CPs are known as nuclear critical points (NCPs) and their positions are almost identical to atomic positions. They

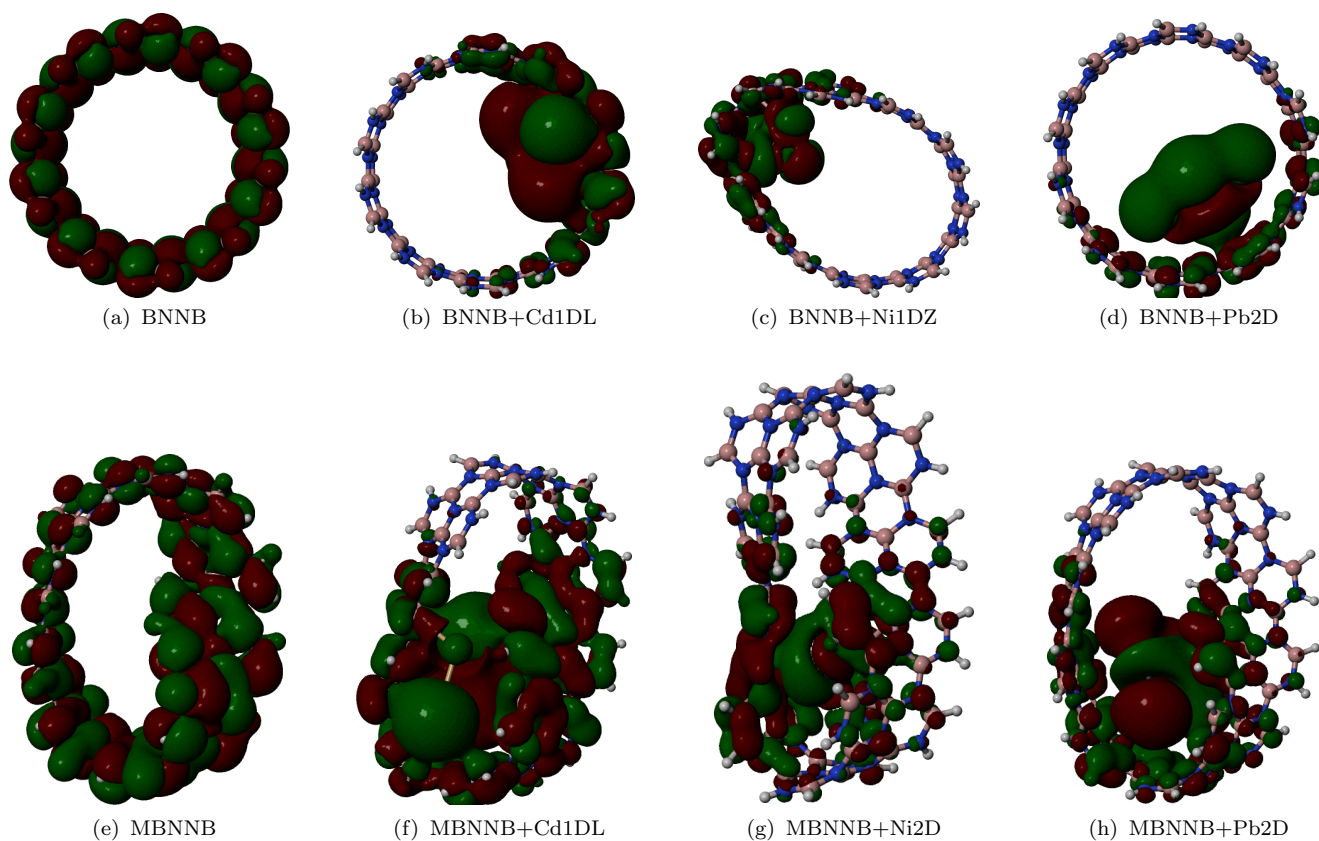


Figure 6: Highest occupied molecular orbital (HOMO) for all systems. Red (green) color represents negative (positive) values. Orbital surfaces rendered with with isovalue equal to 0.001 and with Jmol software [44].

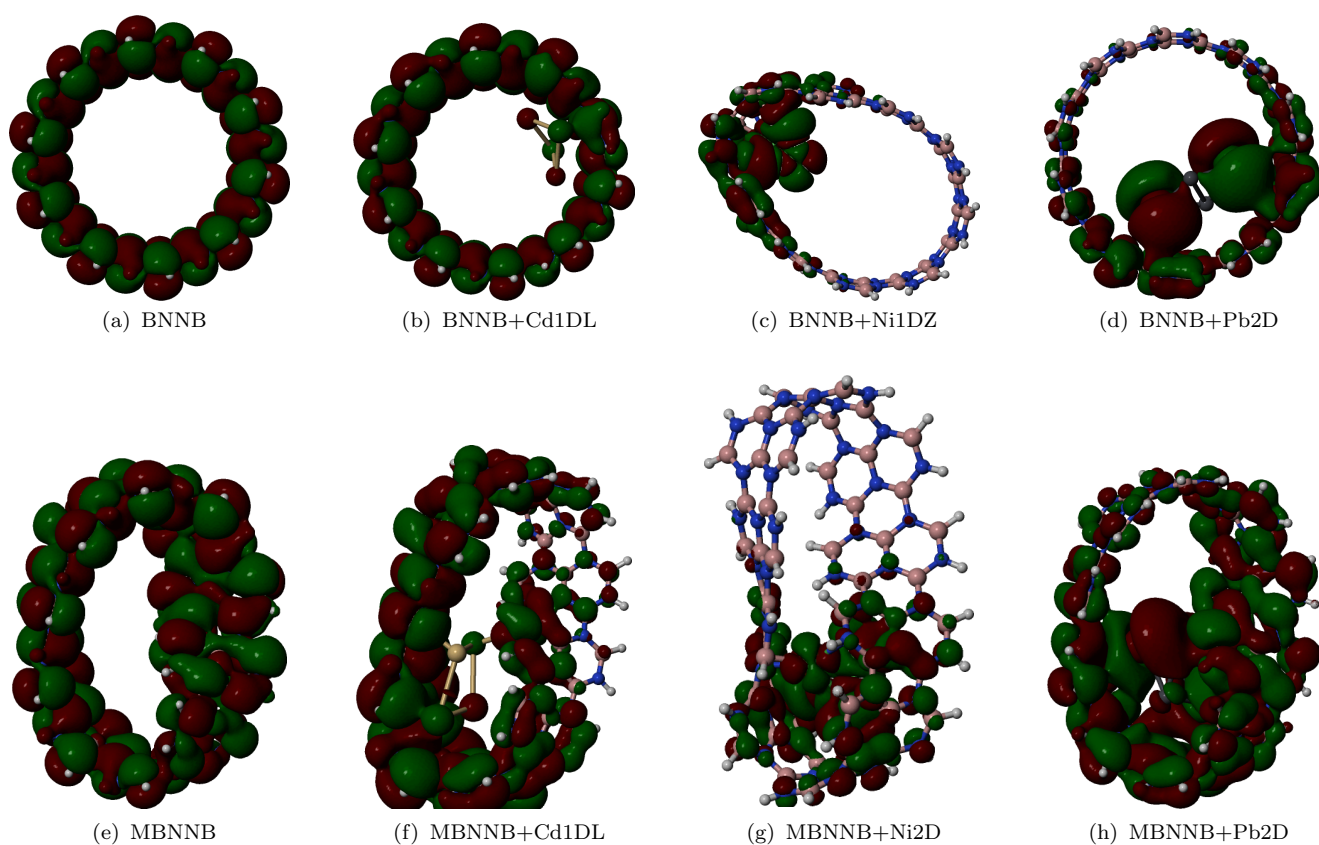


Figure 7: Lowest unoccupied molecular orbital (LUMO) for all systems. Red (green) color represents negative (positive) values. Orbital surfaces rendered with with isovalue equal to 0.001 and with Jmol software [44].

are represented as $(\mathbf{3}, -\mathbf{3})$. If two eigenvalues of the Hessian matrix are negative, the CPs are represented as $(\mathbf{3}, -\mathbf{1})$ and are referred to as bond critical points (BCPs). These BCPs generally appear between atom pairs in electron density analysis and are related to the strength and type of bonds formed. The value of the electron density (ρ) and the sign of its Laplacian ($\nabla^2\rho$) at the $(\mathbf{3}, -\mathbf{1})$ CPs can be related to the strength and type of the bonds [48]. CPs with one negative eigenvalue are represented as $(\mathbf{3}, +\mathbf{1})$ and are called ring critical points (RCPs) because they usually appear in the center of a ring system. Finally, CPs with no negative eigenvalues are represented as $(\mathbf{3}, +\mathbf{3})$ and are called cage critical points (CCPs) because they typically appear in the center of a cage system during electron density analysis.

Diagrams with the 3D distribution of critical points for each complex are shown in Figure 8. The orange dots represent the bond critical points (BCPs), the yellow dots represent the ring critical points (RCPs), and the green dots represent the cage critical points. All the complexes show several critical points, indicating a favorable interaction between the metals and the belts. In all cases, the number of critical points made between the metal nanocluster and the Möbius nanobelts is greater than with the nanobelts alone. This can be associated with the fact that Möbius belts form like small pockets where the metal nanocluster can be docked. The interaction between the Ni₂D nanocluster with the MBNNB is so intense that it pulled both sides of the belt in such a way that new bonds are formed between both sides (see Figure 8(e)). For better visualization of the formed critical points, movies with spinning structures can be downloaded from the Zenodo server [47]. Another confirmation that the strongest interactions are between the Ni nanoclusters and the boron-nitride nanobelts is the lowest bond distances shown in Table 1.

The strength of a bond, whether it is covalent or non-covalent, can be classified by examining the electron density (ρ) and the sign of its Laplacian ($\nabla^2\rho$). A value of ρ greater than 0.20 a.u. indicates a covalent bond, while a value less than 0.10 a.u. indicates a non-covalent bond. Moreover, a bond can be classified as covalent if $\nabla^2\rho$ is less than 0, and as non-covalent if $\nabla^2\rho$ is greater than 0 [48]. The confinement of electron movement is related to the ELF index, which takes values in the range of 0 to 1 [50; 51]. Large values of the

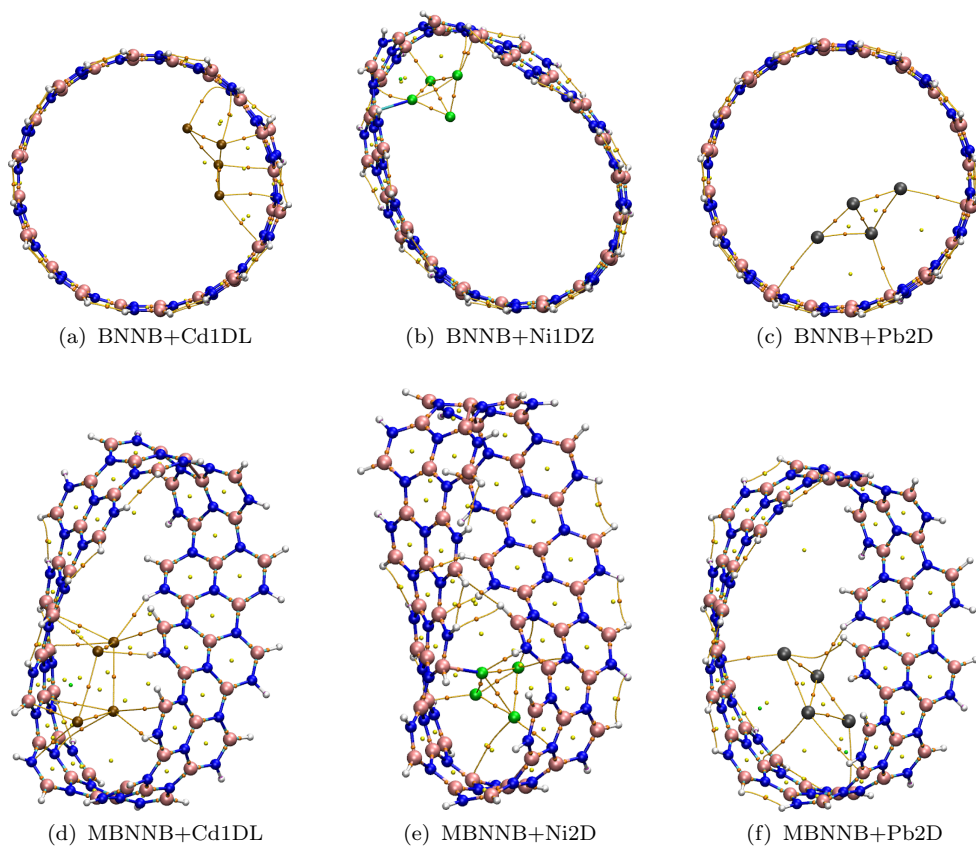


Figure 8: Detected critical points: BCPs (orange dots), RCPs (yellow dots), and CCPs (green dots). Image rendered with VMD software [49].

ELF index indicate that electrons are highly localized, which is indicative of the presence of a covalent bond. The LOL index is another function that is used to identify regions of high localization [52]. Values of the LOL index are also in the range of 0 to 1, with smaller (larger) values typically appearing in the boundary (inner) regions.

Figure 9 shows the electron density (ρ), Laplacian of the electron density ($\nabla^2\rho$), electron localization function (ELF) index, and localized orbital locator (LOL) index at all the detected bond critical points. The maximum number of BCPs for MBNNB is twice that for BNNB, indicating that using Möbius boron–nitride nanobelts to capture heavy metal nanoclusters is a better choice. According to the classification criteria above, higher values of ρ indicate stronger bonds. Figures 9(a), 9(b), 9(e), and 9(f) show that MBNNB made stronger bonds with Ni clusters (green regions) than with the other metals (orange regions for Cd clusters and gray regions for Pb clusters). Even though Cd nanocluster forms more bonds with MBNNB than Ni nanocluster, they have lower values of ρ and $\nabla^2\rho$. The ELF (figures 9(c), and 9(g)) and LOL (figures 9(d), and 9(h)) indexes show that some of the BCPs for Cd nanoclusters have greater values than for Ni and Pb clusters. This higher electron localization of Cd cluster is associated with the HOMO redistribution shown in figures 6(b), and 6(f). The topological analysis confirms that both boron–nitride nanobelts are capable of adsorbing the three heavy metal nanoclusters studied here. Nevertheless, the MBNNB presented greater values for all the descriptors used. In all cases, the Ni nanoclusters are chemisorbed, whereas Cd and Pb nanoclusters are physisorbed.

4. Conclusions

In this work, the interactions of Ni, Cd, and Pb nanoclusters with boron-nitride nanobelts with different geometries were studied within the semiempirical tight binding framework using several methods: best interaction region, geometry optimization, molecular dynamics, electronic property calculations, and topology studies.

The more favorable interaction regions were determined using the automated Interaction Site Screening (aISS) and used as a starting point for the other simulations. All the structures (individual clusters, nanobelts, and complexes) were optimized under extreme

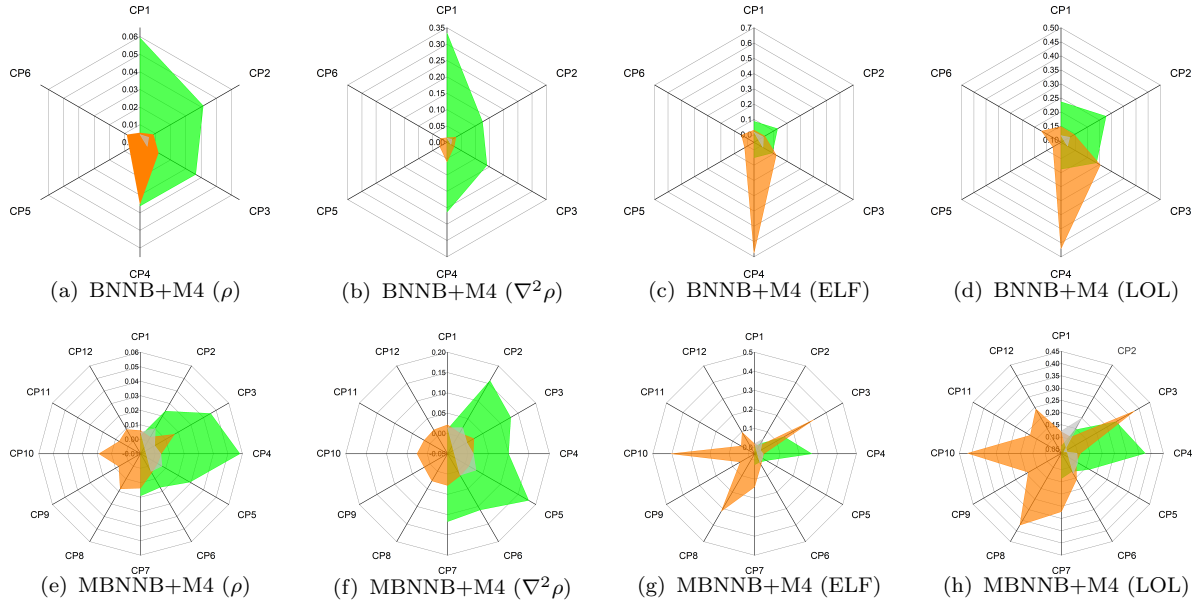


Figure 9: Topology results. The data for Ni clusters is in green, for Cd clusters is in orange and for Pb clusters is in gray.

optimization level to ensure good convergence. The final energy of the optimized structures was used to calculate the binding energy for each complex. From the energy analysis, the Ni nanocluster shows the lower binding energy (most favorable interaction) followed by Cd and Pb nanoclusters. The final geometry for the MBNNB+Ni₂D system shows that the Ni nanocluster pulled the nanobelt sides in such a way that both sides start interacting, creating a closed pocket around the metal nanocluster. To study the complexes' time stability, molecular dynamics simulations were run for a production time of 100 ps, showing that, in all cases, the heavy metals remain bound to the nanobelts.

The electronic calculations showed that the topology of the MBNNB changed the HOMO/LUMO distribution when compared to BNNB as there is a break in symmetry (for BNNB) that induced a redistribution of the orbitals around the twisted region (for MBNNB). The interaction of heavy metals nanocluster produced a further modification of the HOMO/LUMO surfaces, being now redistributed around the region where the metal was located. Due to the metal/nanobelt interaction, the charges of the nanocluster were also modified to a greater extent for the Ni nanocluster than for the other metals.

The topological analysis detected the critical points used to better characterize the type and strength of the interactions. The MBNNB has twice the number of bond critical points than the BNNB system. This is an indicator that using MBNNB to adsorb the heavy metals is a better choice. Comparing the values of the descriptors used (electron density, Laplacian of the electron density, ELF, and LOL indexes) for all the systems, we can conclude that the Ni nanocluster is better adsorbed than the Cd and Pb nanoclusters.

Combining the results from the geometry optimization, the binding energy calculation, and the topological analysis, we can conclude that the Ni nanoclusters are chemisorbed, whereas Cd and Pb nanoclusters are physisorbed in both nanobelts, but this adsorption is more favorable for the Möbius boron-nitride nanobelts.

CRedit authorship contribution statement

C. Aguiar: Investigation, Formal analysis, Writing–original draft, Writing–review & editing. **N. Dattani:** Investigation, Resources, Formal analysis, Writing–original draft, Writing–review & editing. **I. Camps:** Conceptualization, Methodology, Software, Formal analysis, Resources, Writing–review & editing, Supervision, Project administration.

Declaration of competing interest

The authors declare that they have no known competing financial interests or personal relationships that could have appeared to influence the work reported in this paper.

Data availability

Data will be made available on request.

Acknowledgements

We would like to acknowledge financial support from the Brazilian agencies CNPq, CAPES and FAPEMIG. Part of the results presented here were developed with the help of a CENAPAD-SP (Centro Nacional de Processamento de Alto Desempenho em São Paulo)

grant UNICAMP/FINEP–MCT, CENAPAD–UFC (Centro Nacional de Processamento de Alto Desempenho, at Universidade Federal do Ceará), and Digital Research Alliance of Canada (via project bmh-491-09 belonging to Dr. Nike Dattani), for the computational support.

References

- [1] P. Mehndiratta, A. Jain, S. Srivastava, N. Gupta, Environmental pollution and nanotechnology, *Environment and Pollution* 2 (2013) 1 (2013). doi:10.5539/ep.v2n2p49.
- [2] X. Zhang, Q. Huang, F. Deng, H. Huang, Q. Wan, M. Liu, Y. Wei, Mussel-inspired fabrication of functional materials and their environmental applications: Progress and prospects, *Appl. Mater. Today* 7 (2017) 222–238 (2017). doi:10.1016/j.apmt.2017.04.001.
- [3] J. Sardans, F. Montes, J. Peñuelas, Electrothermal atomic absorption spectrometry to determine As, Cd, Cr, Cu, Hg, and Pb in soils and sediments: A review and perspectives, *Soil Sediment Contam.* 20 (2011) 447–491 (2011). doi:10.1080/15320383.2011.571526.
- [4] M. Bali, H. Tlili, Removal of heavy metals from wastewater using infiltration-percolation process and adsorption on activated carbon, *Int. J. Environ. Sci. Te.* 16 (2018) 249–258 (2018). doi:10.1007/s13762-018-1663-5.
- [5] G. A. Engwa, P. U. Ferdinand, F. N. Nwalo, M. N. Unachukwu, Mechanism and health effects of heavy metal toxicity in humans, *IntechOpen*, 2019 (2019). doi:10.5772/intechopen.82511.
- [6] C. Moreno-Castilla, M. A. Álvarez-Merino, M. V. López-Ramón, J. Rivera-Utrilla, Cadmium ion adsorption on different carbon adsorbents from aqueous solutions. effect of surface chemistry, pore texture, ionic strength, and dissolved natural organic matter, *Langmuir* 20 (2004) 8142–8148 (2004). doi:10.1021/la049253m.
- [7] M. Jaishankar, T. Tseten, N. Anbalagan, B. B. Mathew, K. N. Beeregowda, Toxicity, mechanism and health effects of some heavy metals, *Interdiscip. Toxicol.* 7 (2014) 60–72 (2014). doi:10.2478/intox-2014-0009.
- [8] R. Baby, B. Saifullah, M. Z. Hussein, Carbon nanomaterials for the treatment of heavy metal-contaminated water and environmental remediation, *Nanoscale Res. Lett.* 14 (2019) 341 (2019). doi:10.1186/s11671-019-3167-8.
- [9] Y. Wu, H. Pang, Y. Liu, X. Wang, S. Yu, D. Fu, J. Chen, X. Wang, Environmental remediation of heavy metal ions by novel-nanomaterials: A review, *Environ. Pollut.* 246 (2019) 608–620 (2019). doi:10.1016/j.envpol.2018.12.076.
- [10] V. K. Gupta, S. Agarwal, T. A. Saleh, Chromium removal by combining the magnetic properties of iron oxide with adsorption properties of carbon nanotubes, *Water Res.* 45 (2011) 2207–2212 (2011). doi:10.1016/j.watres.2011.01.012.
- [11] A. E. Burakov, E. V. Galunin, I. V. Burakova, A. E. Kucherova, S. Agarwal, A. G. Tkachev, V. K. Gupta, Adsorption of heavy metals on conventional and nanostructured materials for wastewater treatment purposes: A review, *Ecotox. Environ. Safe.* 148 (2018) 702–712 (2018). doi:10.1016/j.ecoenv.2017.11.034.

- [12] M. Bastos, I. Camps, Interactions of lead with carboxyl and hydroxyl-decorated (10, 0) single-walled carbon nanotubes: First-principle calculations, *Appl. Surf. Sci.* 285P (2013) 198–204 (2013). doi:10.1016/j.apsusc.2013.08.036.
- [13] K. Kaneko, C. Ishii, T. Arai, H. Suematsu, Defect-associated microporous nature of fullerene C₆₀ crystals, *J. Phys. Chem.* 97 (1993) 6764–6766 (1993). doi:10.1021/j100128a002.
- [14] M. Bastos, I. Camps, First-principles calculations of nickel, cadmium, and lead adsorption on a single-walled (10,0) carbon nanotube, *J. Mol. Model.* 20 (2014) 2094 (2014). doi:10.1007/s00894-014-2094-y.
- [15] H. Cho, J. H. Kim, J. H. Hwang, C. S. Kim, S. G. Jang, C. Park, H. Lee, M. J. Kim, Single- and double-walled boron nitride nanotubes: Controlled synthesis and application for water purification, *Sci. Rep.* 10 (2020) 7416 (2020). doi:10.1038/s41598-020-64096-z.
- [16] A. O. Maselugbo, H. B. Harrison, J. R. Alston, Boron nitride nanotubes: A review of recent progress on purification methods and techniques, *J. Mater. Res.* 37 (2022) 4438–4458 (2022). doi:10.1557/s43578-022-00672-5.
- [17] V. Dutta, R. Verma, C. Gopalkrishnan, M. H. Yuan, K. M. Batoo, R. Jayavel, A. Chauhan, K. Y. A. Lin, R. Balasubramani, S. Ghotekar, Bio-inspired synthesis of carbon-based nanomaterials and their potential environmental applications: a state-of-the-art review, *Inorganics* 10 (2022) 169 (2022). doi:10.3390/inorganics10100169.
- [18] T. Li, Z. Tang, Z. Huang, J. Yu, A comparison between the mechanical and thermal properties of single-walled carbon nanotubes and boron nitride nanotubes, *Phys. E: Low-Dimens. Syst. Nanostructures* 85 (2017) 137–142 (2017). doi:10.1016/j.physe.2016.08.012.
- [19] J. Yin, J. Li, Y. Hang, J. Yu, G. Tai, X. Li, Z. Zhang, W. Guo, Boron nitride nanostructures: Fabrication, functionalization and applications, *Small* 12 (2016) 2942–2968 (2016). doi:10.1002/smll.201600053.
- [20] L. Vaccarini, C. Goze, L. Henrard, E. Hernández, P. Bernier, A. Rubio, Mechanical and electronic properties of carbon and boron–nitride nanotubes, *Carbon* 38 (2000) 1681–1690 (2000). doi:10.1016/S0008-6223(99)00293-6.
- [21] R. Ansari, F. Sadeghi, S. Ajori, Oscillation characteristics of carbon nanotube molecules along carbon nanotubes under various system parameters, *Europ. J. Mech. A/Solids* 62 (2017) 67–79 (2017).
- [22] A. M. Patki, R. K. Goyal, High performance polyetherketone-hexagonal boron nitride nanocomposites for electronic applications, *J. Mater. Sci.: Mater. Electron.* 30 (2019) 3899–3908 (2019). doi:10.1007/s10854-019-00675-9.
- [23] H. Oh, J. Kim, Fabrication of polymethyl methacrylate composites with silanized boron nitride by in-situ polymerization for high thermal conductivity, *Compos. Sci. Technol.* 172 (2019) 153–162 (2019).

- doi:10.1016/j.compscitech.2019.01.021.
- [24] R. N. Muthu, S. Rajashabala, R. Kannan, Hexagonal boron nitride (h-BN) nanoparticles decorated multi-walled carbon nanotubes (MWCNT) for hydrogen storage, *Renew. Energ.* 85 (2016) 387–394 (2016). doi:10.1016/j.renene.2015.06.056.
- [25] M. Jedrzejczak-Silicka, M. Trukawka, M. Dudziak, K. Piotrowska, E. Mijowska, Hexagonal boron nitride functionalized with Au nanoparticles—properties and potential biological applications, *Nanomaterials* 8 (2018) 605 (2018). doi:10.3390/nano8080605.
- [26] D. Maiti, X. Tong, X. Mou, K. Yang, Carbon-based nanomaterials for biomedical applications: A recent study, *Front. Pharmacol.* 9 (2019) 01401 (2019). doi:10.3389/fphar.2018.01401.
- [27] D. Gonzalez-Ortiz, C. Salameh, M. Bechelany, P. Miele, Nanostructured boron nitride-based materials: synthesis and applications, *Mater. Today Adv.* 8 (2020) 100107 (2020). doi:10.1016/j.mtadv.2020.100107.
- [28] R. Madeira, I. Camps, First-principles calculations of nickel, cadmium, and lead nanoclusters adsorption on single-wall (10,0) boron-nitride nanotube, *Appl. Surf. Sci.* 573 (2022) 151547 (2022). doi:10.1016/j.apsusc.2021.151547.
- [29] E. A. Turhan, A. E. Pazarçeviren, Z. Evis, A. Tezcaner, Properties and applications of boron nitride nanotubes, *Nanotechnology* 33 (2022) 242001 (2022). doi:10.1088/1361-6528/ac5839.
- [30] A. Khalid, P. Ahmad, A. Khan, M. U. Khandaker, I. Kebaili, M. Alam, I. U. Din, S. Muhammad, Z. Razzaq, I. U. Rehman, H. A. Abbasi, D. Hayat, Cytotoxic and photocatalytic studies of hexagonal boron nitride nanotubes: a potential candidate for wastewater and air treatment, *RSC Advances* 12 (2022) 6592–6600 (2022). doi:10.1039/d2ra00300g.
- [31] B. L. Merner, L. N. Dawe, G. J. Bodwell, 1,1,8,8-tetramethyl[8](2,11)teropyrenophane: Half of an aromatic belt and a segment of an (8,8) single-walled carbon nanotube, *Angew. Chem. Int. Ed.* 48 (2009) 5487–5491 (2009). doi:10.1002/anie.200806363.
- [32] L. S. Barbosa, B. C. de Almeida, E. Moreira, D. L. Azevedo, First-principle investigation of boron nitride nanobelt, *Comput. Theor. Chem.* 1208 (2022) 113571 (2022). doi:10.1016/j.comptc.2021.113571.
- [33] G. Povie, Y. Segawa, T. Nishihara, Y. Miyauchi, K. Itami, Synthesis of a carbon nanobelt, *Science* 356 (2017) 172–175 (2017). doi:10.1126/science.aam8158.
- [34] K. Y. Cheung, S. Gui, C. Deng, H. Liang, Z. Xia, Z. Liu, L. Chi, Q. Miao, Synthesis of armchair and chiral carbon nanobelts, *Chem* 5 (2019) 838–847 (2019). doi:10.1016/j.chempr.2019.01.004.
- [35] Z. Xia, S. H. Pun, H. Chen, Q. Miao, Synthesis of zigzag carbon nanobelts through scholl reactions, *Angew. Chemie.* 133 (2021) 10399–10406 (2021). doi:10.1002/ange.202100343.
- [36] Virtual NanoLab - Atomistix ToolKit. QuantumWise. v2017.1 (2017).
- [37] C. Bannwarth, E. Caldeweyher, S. Ehlert, A. Hansen, P. Pracht, J. Seibert, S. Spicher, S. Grimme,

- Extended tight-binding quantum chemistry methods, *WIREs Comput. Mol. Sci.* 11 (2020) e1493 (2020). doi:10.1002/wcms.1493.
- [38] S. Grimme, C. Bannwarth, P. Shushkov, A robust and accurate tight-binding quantum chemical method for structures, vibrational frequencies, and noncovalent interactions of large molecular systems parametrized for all spd-block elements ($Z=1-86$), *J. Chem. Theory Comput.* 13 (2017) 1989–2009 (2017). doi:10.1021/acs.jctc.7b00118.
- [39] C. Plett, S. Grimme, Automated and efficient generation of general molecular aggregate structures, *Angew. Chem. Int. Ed.* 62 (2022). doi:10.1002/anie.202214477.
- [40] S. Grimme, C. Bannwarth, E. Caldeweyher, J. Pisarek, A. Hansen, A general intermolecular force field based on tight-binding quantum chemical calculations, *The Journal of Chemical Physics* 147 (2017) 161708 (2017). doi:10.1063/1.4991798.
- [41] C. Bannwarth, S. Ehlert, S. Grimme, GFN2-xTB—An accurate and broadly parametrized self-consistent tight-binding quantum chemical method with multipole electrostatics and density-dependent dispersion contributions, *J. Chem. Theory Comput.* 15 (2019) 1652–1671 (2019). doi:10.1021/acs.jctc.8b01176.
- [42] A. V. Marenich, S. V. Jerome, C. J. Cramer, D. G. Truhlar, Charge Model 5: an extension of Hirshfeld population analysis for the accurate description of molecular interactions in gaseous and condensed phases, *Journal of Chemical Theory and Computation* 8 (2012) 527–541 (2012). doi:10.1021/ct200866d.
- [43] T. Lu, F. Chen, Multiwfn: A multifunctional wavefunction analyzer, *J. Comput. Chem.* 33 (2012) 580–592 (2012). doi:10.1002/jcc.22885.
- [44] Jmol: An open-source Java viewer for chemical structures in 3D. <http://www.jmol.org/>.
- [45] D. H. Everett, Manual on Definitions, Terminology and Symbols in Colloid and Surface Chemistry (internet version), Vol. 31, IUPAC. Division of Physical Chemistry, 2001 (2001). doi:10.1351/pac197231040577.
- [46] R. F. W. Bader, *Atoms in Molecules: A Quantum Theory*, Clarendon Press, 1994 (1994).
- [47] C. Aguiar, N. Dattani, I. Camps, (VIDEOS) Möbius boron–nitride nanobelts interacting with heavy metal nanoclusters (2023). doi:10.5281/zenodo.7662326.
- [48] C. F. Matta, R. J. Boyd, *The Quantum Theory of Atoms in Molecules: From Solid State to DNA and Drug Design*, John Wiley & Sons, 2007 (2007).
- [49] W. Humphrey, A. Dalke, K. Schulten, VMD: Visual molecular dynamics, *Journal of Molecular Graphics* 14 (1996) 33–38 (fe 1996). doi:10.1016/0263-7855(96)00018-5.
- [50] A. D. Becke, K. E. Edgecombe, A simple measure of electron localization in atomic and molecular systems, *The Journal of Chemical Physics* 92 (1990) 5397–5403 (1990). doi:10.1063/1.458517.

- [51] K. Koumpouras, J. A. Larsson, Distinguishing between chemical bonding and physical binding using electron localization function (ELF), *J. Phys.: Condens. Matter* 32 (2020) 315502 (2020). doi:10.1088/1361-648X/ab7fd8.
- [52] H. L. Schmider, A. D. Becke, Chemical content of the kinetic energy density, *J. Mol. Struct.: THEOCHEM* 527 (2000) 51–61 (2000). doi:10.1016/S0166-1280(00)00477-2.